Earth Planet. Sci. Lett. 642 (2024) 118868

Contents lists available at ScienceDirect

Earth and Planetary Science Letters

journal homepage: www.elsevier.com/locate/epsl

Mg and Fe isotope compositions of mid-ocean ridge basalts modified by Mg-Fe inter-diffusion during melt transport

Xiao-Ning Liu (刘效宁) [a,*], Remco C. Hin [a,b], Christopher D. Coath [a], Tim Elliott [a]

[a] Bristol Isotope Group, School of Earth Science, University of Bristol, Bristol BS8 1RJ, UK
[b] Institute of Environmental Geology and Geoengineering, Consiglio Nazionale delle Ricerche (CNR), Via Sandro Botticelli 23, 20133 Milan, Italy

ARTICLE INFO

Edited by: DR J BADRO

Keywords:
Mg isotope
Fe isotope
Mid-ocean ridge basalt
Mg-Fe inter-diffusion
Kinetic isotope fractionation

ABSTRACT

We analysed forty-nine, hand-picked, mid-ocean ridge basalt (MORB) glasses for their Mg isotopic compositions using a high-precision, critical mixture double-spiking approach. Additionally, the Fe isotopic compositions of a subset (twenty-two) of these samples were measured. Samples from the East Pacific, Mid-Atlantic, South East Indian and East Scotia ridges have average δ^{26}Mg ~ −0.21 ‰ and δ^{57}Fe ~0.10 ‰, while those from the ultra-slow spreading Gakkel and South West Indian ridges have lighter Mg isotope compositions, δ^{26}Mg as low as ~ −0.32 ‰, and heavier Fe isotope compositions, δ^{57}Fe up to 0.25 ‰. Overall, the samples show a striking negative correlation between δ^{26}Mg and δ^{57}Fe. Few MORB have δ^{26}Mg as high as predicted by equilibrium models of melting and differentiation; in complementary fashion, measured δ^{57}Fe are typically higher than modelled, equilibrium values. Furthermore, we show that the slope of ^{26}Mg/^{24}Mg and ^{25}Mg/^{24}Mg covariations in MORB is consistent with kinetic not equilibrium fractionation. These observations identify an important diffusive control on both Mg and Fe isotopic compositions of MORB. Fractional transport of melt beneath ridges juxtaposes low Mg/Fe fractional melts from depth with high Mg/Fe residues at the top of the melting column. We argue that diffusively limited, partial Mg-Fe exchange between melt and peridotite through which it migrates leads to melts becoming isotopically lighter in Mg and heavier in Fe. Low melt rock ratios from sub-adiabatic melting beneath the slowest spreading ridges result in the greatest diffusive exchange between peridotite and melt en route to surface.

1. Introduction

Terrestrial peridotites have Mg isotopic compositions that are subtly heavier than bulk chondritic values (Hin et al., 2017; Liu et al., 2023). Given accessible peridotites are widely used to provide a compositional estimate of the mantle as a whole, especially for major mineral forming elements such as Mg, this observation implies that bulk Earth has super-chondritic ^{26}Mg/^{24}Mg. Since Mg is a relatively refractory, lithophile element, this is a surprising finding but one with significant ramifications for the formation of Earth. For example, in order to explain its Mg isotopic composition, Hin et al. (2017) argued that the planetesimals that ultimately formed Earth suffered extensive (some 40 % by mass), evaporative loss during their accretion. However, analysed mantle peridotites are mainly from the continental lithosphere and so it is critical to test if the volumetrically dominant, convecting mantle also has an isotopically heavy Mg isotopic composition. Since the convecting mantle is mainly sampled by the melts it produces, this task requires not only precise analyses but also an accurate inversion for isotopic fractionation during the melting process (see Stracke et al., 2018; Soderman et al., 2022). To this end we present a combination of new, high-precision analyses of mid-ocean ridge basalts (MORB) interpreted with refined parameters for quantifying melt fractionation of Mg isotope ratios (Liu et al., 2022; Liu et al., 2023).

A previous, extensive study of the magnesium isotope compositions of MORB (Teng et al., 2010) yielded data that form a single population with δ^{26}Mg of −0.24 ± 0.01 ‰ (2se). This value is similar to the Mg isotope ratio determined in several studies of peridotites (δ^{26}Mg of ~ −0.24 ‰, e.g., Teng et al., 2010; Liu et al., 2023). While this observation is consistent with an earlier assessment of insignificant melt-olivine Mg isotope fractionation, within the uncertainty of the sample-standard bracketing method used (Teng et al., 2007), more recent, direct determination of this parameter (Liu et al., 2022) predicts that MORB should have δ^{26}Mg approximately 0.05 ‰ higher than its source through equilibrium partial melting (Liu et al., 2023). Some higher precision

* Corresponding author.
E-mail address: Xiaoning.liu@bristol.ac.uk (X.-N. Liu (刘效宁)).

https://doi.org/10.1016/j.epsl.2024.118868
Received 13 December 2023; Received in revised form 18 June 2024; Accepted 25 June 2024
Available online 14 July 2024

MORB measurements (Hin et al., 2017; Liu et al., 2022) also show Mg isotopic compositions within error of peridotites (from −0.224 ‰ to −0.256 ‰, ±0.020 ‰) rather than the isotopically heavier values of model predictions. This preliminary finding needs to be substantiated with additional, high precision measurements, but the inconsistency suggests the involvement of another process responsible for fractionating Mg isotope compositions during magma genesis. Otherwise, a scenario of a different Mg isotopic composition of the lithosphere and asthenosphere needs to be considered.

One possible explanation for the unexpectedly low δ^{26}Mg of MORB is kinetic isotope fractionation during diffusional exchange of Fe and Mg between mantle and percolating melts that are out of Mg-Fe equilibrium (Liu et al., 2023). A similar inference has previously been made to explain why the Fe isotopic compositions of some bulk peridotite analyses exceed those predicted from equilibrium melt-solid fractionation (e.g. Weyer and Ionov, 2007; Poitrasson et al., 2013). Large and inversely correlated variations of δ^{57}Fe and δ^{26}Mg in olivine phenocrysts, measured both in situ (Sio et al., 2013; Oeser et al., 2015) and in bulk analyses (e.g., Dauphas et al., 2010; Teng et al., 2011) also strongly argue for inter-diffusional Fe-Mg exchange between minerals and melt. While this previous work has primarily focused on the influence of diffusive exchange on the composition of the solid phase, there will be a complementary disturbance of the Fe and Mg isotope compositions of the associated melt. To assess better this possible influence on the Mg isotopic compositions of MORB, we additionally analysed some samples for their Fe isotope compositions.

Diffusive, kinetic isotope fractionation can also be distinguished from equilibrium isotope fractionation by subtle differences in the covariation of mass dependent fractionations of ^{26}Mg/^{24}Mg and ^{25}Mg/^{24}Mg (e.g. Young and Galy, 2004). This effect can be quantified by the parameter $\Delta^{25}Mg' = \delta^{25}Mg' - \beta \times \delta^{26}Mg'$ where $\beta = 0.521$ is for equilibrium and $\beta = 0.511$ for kinetic fractionation (see Young and Galy, 2004, where $\delta^{x}Mg' = \ln[(^{x}Mg/^{24}Mg)_{sample}/(^{x}Mg/^{24}Mg)_{reference}]$, $x = 25$ or 26). In practice this is analytically challenging in the case of MORB since the anticipated variations in $\Delta^{25}Mg'$ are only a few parts per million (ppm), considering the relatively minor variations in $\delta^{26}Mg'$ (less than 0.2 ‰). However, we have combined application of our critical mixture double-spike method (see Methods and Coath et al., 2017) with multiple repeat measurements of high intensity Mg beams to determine $\Delta^{25}Mg'$ (e.g. Luu et al., 2019, Gregory et al., 2020) to obtain sufficient precision in order to use this additional constraint.

2. Samples

2.1. MORB samples and tectonic settings

We analysed forty-nine MORB samples for their Mg isotopic compositions, and additionally, we measured the Fe isotope composition of twenty-two of these samples. We include samples from the East Pacific Rise (EPR) (Niu et al., 1996; 1999; Regelous et al., 1999; Sims et al., 2002), the Mid-Atlantic Ridge (MAR) (Niu and Batiza 1994; Regelous et al., 2009), the South West Indian Ridge (SWIR) (Robinson et al., 1996), the South East Indian Ridge (SEIR) (Mahoney et al., 2002), the Gakkel Ridge (Richter et al., 2020, 2021) and the (back-arc) East Scotia Ridge (Fretzdorff et al., 2002). These localities span a wide range of spreading rates and settings, providing broad coverage of the mid-ocean ridge system worldwide (Fig. S1). We only analysed MORB from ridge segments uninfluenced by hotspots, as indicated by their axial depths >2500 m (e.g. Klein and Langmuir, 1987).

A summary of the geochemical characteristics of the samples is shown in Fig. 1. More details of these previously well-studied samples can be found in supplementary materials and the references cited above. Our samples span a range of MgO from ~10 wt.% to ~5 wt.%, with other major element variations following a liquid line of descent involving fractional crystallisation of olivine, clinopyroxene, and plagioclase (in mass ratios of 2:1:1, Fig. 1a). The samples are mainly geochemically 'depleted', e.g. values less than unity for La/Sm normalised to a primitive mantle value, $(La/Sm)_N$, and unradiogenic $^{87}Sr/^{86}Sr$ (Fig. 1b). These features reflect an upper mantle source that has suffered (ancient) loss of a melt component and is broadly complementary to the continental crust. Our samples encompass global-scale differences in radiogenic isotopic compositions between samples from different ocean basins, the so-called DUPAL anomaly (Dupré and Allégre 1983; Hart et al., 1984). This is manifest in generally more radiogenic Sr isotope ratios (and less radiogenic Pb isotope ratios) in Indian Ocean MORB relative to the Pacific (Dupré and Allègre, 1983; Fig. 1b). Our dataset also includes some more 'enriched' compositions, typical of the short-length scale geochemical heterogeneity in the ridge system. We identify four such 'enriched' samples, two EPR, one SEIR and one Gakkel Ridge sample that have markedly higher $(La/Sm)_N$ and $^{87}Sr/^{86}Sr$ than other MORB from the same section of ridge. These samples are indicated with crosses in the figures.

2.2. Transect through a quenched pillow rim

We also checked for Mg isotopic variability at the margin of a basaltic

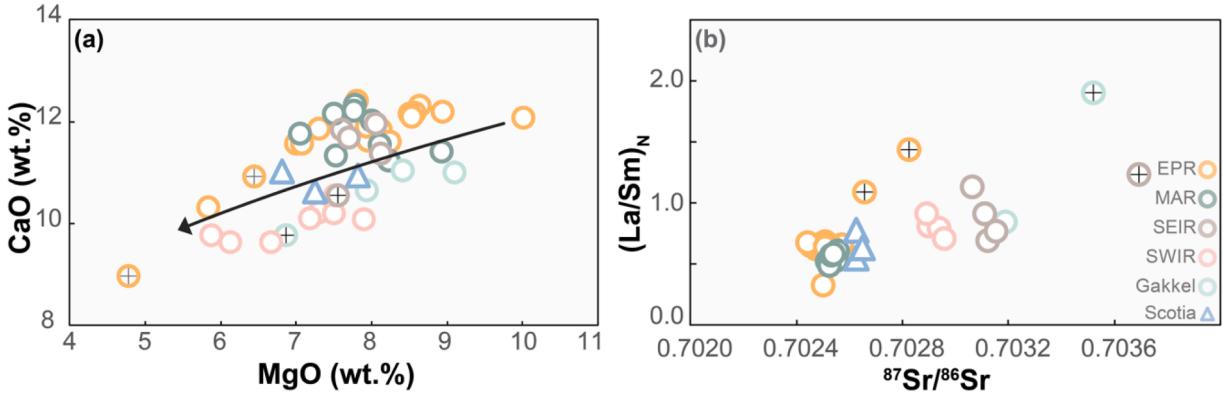

Fig. 1. Characteristic geochemical variations of the MORB samples analysed in this study. (a) MgO vs. CaO illustrates magma differentiation, with the black arrow indicating the vector of fractional crystallisation of an assemblage 20 %Olivine + 10 %Clinopyroxene + 10 %Plagiolcase. (b) $^{87}Sr/^{86}Sr$ vs. primitive mantle normalised La/Sm, $(La/Sm)_N$. Variable Sr isotopic compositions reflect mantle source heterogeneity. Equally $(La/Sm)_N$ dominantly records mantle source compositions but is also be influenced by different degrees of melting. Samples with elevated $^{87}Sr/^{86}Sr$ and $(La/Sm)_n$ are frequently described as 'enriched'. For EPR, SEIR and the Gakkel Ridge, some samples are markedly more enriched than others from the same location. These locally 'enriched' samples are marked with crosses and thus identified in other plots. Primitive mantle composition after Palme and O'Neill (2014).

pillow. The thermal gradients at pillow rims are some of the more extreme in natural magmatic samples. This has the potential to give rise to thermal (or Soret) diffusion, albeit rapid quenching should significantly limit its influence in generating compositional differences. Nonetheless the notable magnitude of isotopic fractionations caused by thermal diffusion, ~7 ‰ in $^{26}Mg/^{24}Mg$ across a temperature difference of 100 °C (e.g., Richter et al., 2008; Huang et al., 2010), encouraged us to assess empirically its possible effect on the Mg isotopic compositions of MORB. Hence we also sampled a pillow margin, in a direction parallel to the thermal gradient on eruption, from the exterior of the quenched glass rim into the more slowly cooled, holocrystalline interior (Fig. 2a and b). Four samples (about 0.4 mg for each) were micro-drilled, every ~ 1.5 cm (sampling positions indicated in Fig. 2a).

3. Methods

All bulk samples studied comprised glass fragments from the naturally quenched rims of pillow basalts. About ten milligrams of MORB glass were hand-picked under an optical, binocular microscope with the criteria of total transparency, clean surfaces and obvious glassy lustre to guarantee sample freshness and avoid crystal contamination. The picked glassy fragments were cleaned in an ultrasonic bath with acetone and 18 Mohm.cm water three times, separately. The pillow rim samples were micro-drilled following the procedure previously reported in Liu et al. (2022). All samples were digested in 3:1 ultra-pure concentrated HNO_3-HF solutions in closed 15 ml Savillex PFA beakers at 150 °C on a hotplate. Ultra-pure, concentrated HCl was then used to attack insoluble fluorides after the HNO_3-HF solution was dried down. After complete digestion, samples were separated into two aliquots for the Mg and Fe isotope analysis, respectively.

3.1. Mass-dependent Mg isotope analysis

The full procedures of mass-dependent Mg isotope analysis using critical mixture double-spiking are given in our previous publications (Hin et al., 2017; Liu et al., 2022, 2023). Briefly, Mg was purified through cation exchange chromatography (Bio-Rad AG50W-X12 resin). Mg isotope analysis was performed on a Thermo-Finnigan Neptune (serial number 1020) multi-collector inductively coupled plasma mass spectrometer (MC-ICPMS) under medium resolution mode ($M/\Delta M \geq$ 4000, 5–95 % peak height definition). Jet sample and H skimmer cones were used. Sample solution was introduced into the mass spectrometer with Savillex PFA nebuliser and Apex HF (Element Inc.). Instrument mass-bias was corrected with the critical mixture double-spike

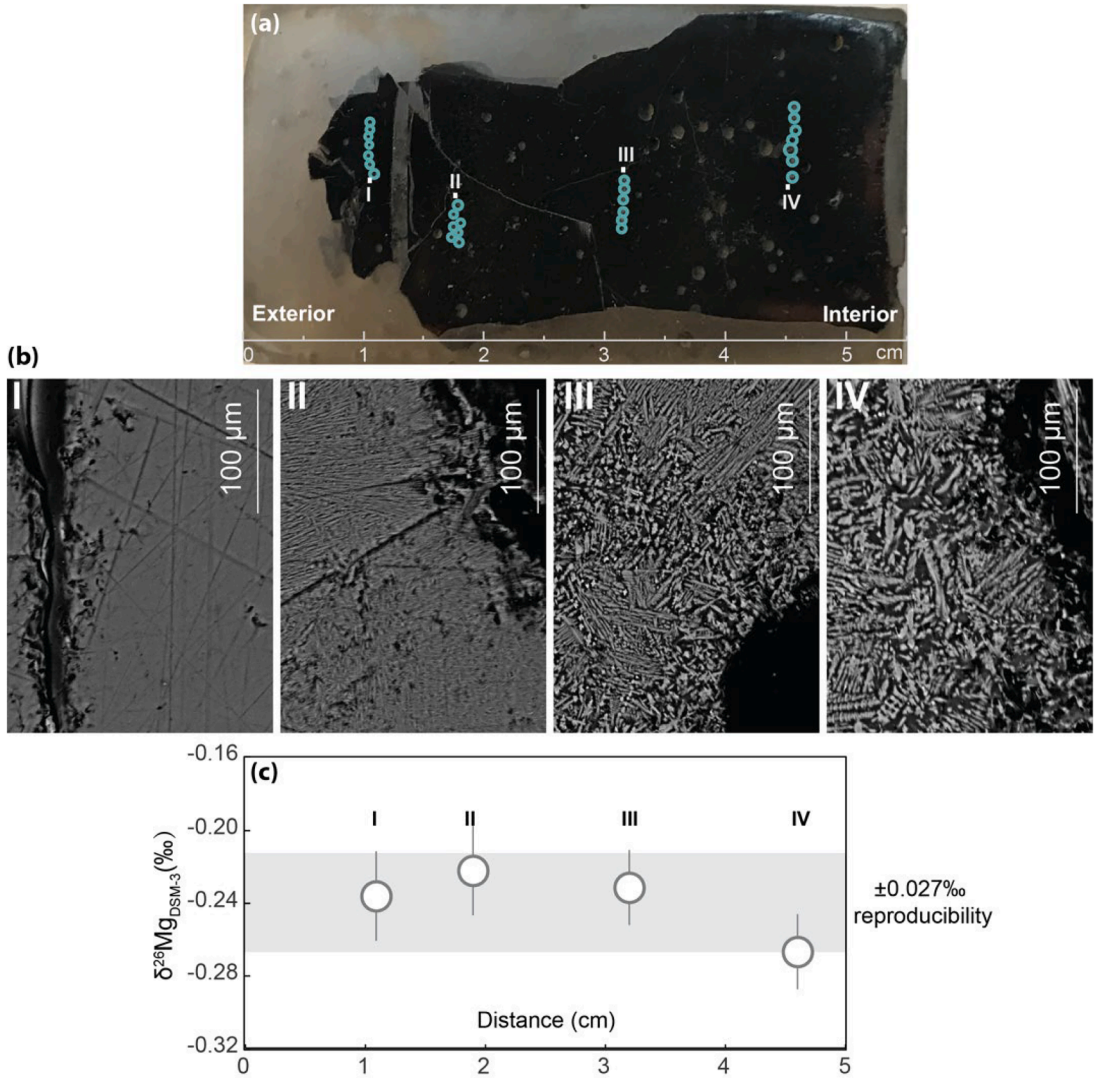

Fig. 2. (a) Optical and (b) BSE images of locations across the quenched margin of a pillow basalt (exterior on left hand side). A clear transition from glassy to microcrystalline texture is evident in (b). The green circles in (a) represent the locations of spots drilled for analysis; each sample is composed of a series of drilled spots. (c) Magnesium isotope ratios across the pillow margin from sample locations marked in (a), showing no significant isotopic variation across the pillow margin.

technique (Coath et al., 2017; Hin et al., 2017). Mg isotope data are reported as $\delta^{26}Mg_{DSM-3}$ (the relative difference of $^{26}Mg/^{24}Mg$ between sample and reference standard DSM-3), subsequently abbreviated as $\delta^{26}Mg$. The long-term reproducibility of our Mg isotope analyses is ±0.027 ‰ (2 s.d., $\delta^{26}Mg$) (Liu et al., 2022). Analyses of various rock standards are given in Liu et al. (2023), who furthermore justified the use of 2se uncertainties as a proxy of reproducibility for Mg isotope compositions obtained by critical mixture double-spiking, an approach that we will follow here.

3.2. Determination of $\Delta^{25}Mg'$

Mg was purified through the column chemistry described above. The analysis followed the protocols of Gregory et al. (2020). In brief, the measurements were performed on a Thermo-Finnigan Neptune MC-ICPMS (serial number 1002) under low resolution ($M/\Delta M \geq 500$, 5–95 % peak height definition). Jet sample cone and H skimmer cone were used. Sample solution was introduced into the mass spectrometer via the combination of a Savillex PFA nebuliser and Apex IR (Element Inc.). Sample solutions had Mg concentrations of 2 μg/ml, yielding ~240 V beams of $^{24}Mg^{+}$ with 10^{10} Ω feedback resistors. Magnesium isotope ratios are externally normalised to bracketing solutions of Mg separated from the rock standard JP-1 and then used to calculate $\Delta^{25}Mg'_{JP\text{-}1} = \delta^{25}Mg'_{JP\text{-}1} - \beta \times \delta^{26}Mg'_{JP\text{-}1}$, using $\beta = 0.521$ (equilibrium isotope fractionation parameter). We use JP-1 as the reference material instead of DSM-3 to provide a direct comparison of peridotite and melts without introducing additional uncertainty of bracketing with an intermediate reference. Note any Mg isotope data reported against JP-1 has subscript

Table 1
Mg and Fe isotope compositions of the MORB samples.

	Latitude	Longitude	MgO (wt.%)	$\delta^{26}Mg_{DSM-3}$ (‰)	2 s.e.	$\delta^{57}Fe_{IRMM014}$ (‰)	2 s.d.	$\Delta^{25}Mg'_{JP\text{-}1}$ (ppm)	2 s.e.
East Pacific Ridge									
PH54-3	10.499	−103.510	6.99	−0.210	0.027				
PH77-6	10.432	−103.850	5.84	−0.176	0.027				
PH103-2[E]	11.367	−103.780	4.78	−0.177	0.027				
PH108-1[E]	11.342	−103.794	6.44	−0.253	0.027				
2352-2	9.557	−104.249	7.80	−0.196	0.017				
2355-8	9.764	−104.277	7.95	−0.237	0.017				
2356-7	9.682	−104.265	8.12	−0.192	0.017				
2361-6	9.652	−104.260	8.64	−0.235	0.024				
2370-6	9.792	−104.284	8.24	−0.204	0.024				
2372-1	9.843	−104.292	8.57	−0.229	0.031				
2392-9			8.50	−0.233	0.031				
2497-1B	9.888	−104.297	7.97	−0.193	0.024				
2504-1	9.838	−104.291	8.53	−0.206	0.017	0.111	0.021	1.2	1.0
2752-6	9.838	−104.291	8.94	−0.207	0.017	0.119	0.029		
4202_4	9.847	−104.293	7.95	−0.211	0.031				
4205_6	9.786	−104.284	7.94	−0.231	0.031				
62-1	18.350	113.380	7.30	−0.178	0.023				
64-2	18.180	113.350	7.08	−0.179	0.025				
D20-2	8.373	−103.660	10.01	−0.215	0.024				
Mid-Atlantic Ridge									
D12–25			8.20	−0.217	0.024				
D12-29	−25.700	−13.911	8.22	−0.226	0.018	0.131	0.061	1.4	1.0
D14-1	−25.775	−13.918	7.05	−0.204	0.024				
D18-1	−26.020	−13.868	7.78	−0.219	0.024				
D18-2	−26.020	−13.868	7.76	−0.205	0.024				
D19-1	−26.014	−13.844	8.00	−0.207	0.023	0.079	0.062	1.2	1.0
D21-1	−26.118	−13.862	7.50	−0.207	0.024				
D23-7	−26.332	−13.794	7.53	−0.239	0.024				
D25-1	−26.471	−13.772	8.10	−0.221	0.024				
D27-3	−26.493	−13.755	8.92	−0.216	0.021	0.114	0.072	0.4	1.0
Back-arc, East Scotia Ridge									
110DS_3	−58.737	−29.867	6.81	−0.204	0.019				
106DS_1	−57.825	−29.933	7.82	−0.215	0.020				
WX54B	−58.383	−29.954	7.25	−0.219	0.023				
Southeast Indian Ridge									
78-2	−44.830	94.830	8.05	−0.188	0.050	0.109	0.105		
100-1	−47.630	101.530	7.60	−0.217	0.043	0.126	0.070		
115-3	−49.230	105.870	7.70	−0.174	0.050	0.139	0.016		
144-04	−50.010	115.210	8.11	−0.227	0.050	0.141	0.087		
145-1[E]	−49.270	116.720	7.55	−0.264	0.022	0.207	0.054	0.9	1.3
Southwest Indian Ridge									
4/9m(1)	−31.795	57.557	6.66	−0.269	0.017	0.182	0.054	1.1	1.1
4/12a(1)	−31.795	57.557	7.30	−0.237	0.020	0.170	0.043		
4/13c			7.50	−0.255	0.020	0.176	0.055		
5/15g	−31.773	57.642	7.51	−0.241	0.025	0.148	0.043		
7/20a	−31.782	57.593	6.13	−0.312	0.020	0.234	0.048	1.4	1.1
8/26f(1)	−31.838	57.527	5.87	−0.266	0.024	0.213	0.072		
9/30a			7.18	−0.266	0.022	0.201	0.063		
12/37f(1)			7.89	−0.286	0.018	0.197	0.052	2.0	0.8
Gakkel Ridge									
D8	82.899	−6.243	8.41	−0.219	0.043	0.146	0.056		
D36[E]	85.263	12.406	6.86	−0.269	0.022	0.251	0.021	2.3	1.1
D59	86.462	71.008	7.93	−0.278	0.050	0.154	0.038		
PS 59	86.673	46.858	9.10	−0.313	0.022	0.234	0.033	3.0	1.2

[E]indicates 'enriched' MORB samples (as defined in text and caption to Fig. 1).

'JP-1', otherwise Mg isotope data are reported against DSM-3. The reported data (Table 1) are the average of around 40 repeats and their 2 s.e. uncertainties, where each repeat consists of 24 cycles with 8.4 s integration time for every cycle, i.e., in total 2.24 h integration time for each sample. Measurements of the USGS rock reference material BHVO-2 against DSM-3 resulted in $\Delta^{25}Mg'_{DSM\text{-}3} = 2.9 \pm 1.1$ ppm (2 s.e., 38 repeats), which agrees with the value reported in the literature (2.7 ± 1.8 ppm, Luu et al., 2019). Further details can be found in the supplementary materials.

3.3. Mass dependent Fe isotope analysis

Anion exchange chromatography (Bio-Rad AG1-X8 resin) was used to purify Fe. Detailed protocols can be found in the supplementary materials. Yields of the Fe column chemistry were monitored based on collected 'splits' before and after the sample aliquot in each column and were over 99.5 % for all samples. The Fe blank of the full chemical procedure is less than 10 ng.

Fe isotope analysis was performed on a Thermo-Finnigan Neptune MC-ICPMS (serial no. 1020). Due to prominent, molecular interferences in this part of the mass spectrum (Fig. S2), robust Fe isotope measurements require a slightly higher mass resolution than for Mg. We normally used a mass resolution over 6000 ($M/\Delta M > 6000$, 5–95 % peak height definition). This mass-resolution is slightly lower than typically reported in the literature studies of Fe isotope measurements, so to document clearly that this is not a problem we made some repeat measurements using a higher mass resolution ($M/\Delta M$ of 8000, 5–95 % peak height definition). The Fe isotope measurements performed at different mass resolutions yielded consistent outcomes (see supplementary material for details).

The sample solution was introduced into the instrument via a Savillex PFA nebuliser and Apex HF (Element Inc.) with an uptake rate of ~40 µl/min. A combination of standard sample and H skimmer cones were used. The sample gas flow (argon) was reduced to 0.9 L/min, from the typical value ~1.1 L/min that yields maximum beam intensity, to decrease the intensities of interfering species (e.g., $^{40}Ar^{14}N^+$, $^{40}Ar^{16}O^+$, etc.). Meanwhile, a concentrated sample solution of 5 µg/ml Fe solution was used to boost the Fe peaks intensities relative to interferences. Instrumental mass-bias was calibrated via sample-standard bracketing, which proved sufficiently reproducible for our purposes. The concentration differences between samples and bracketing reference (IRMM014) were within ±5 %.

Samples were measured 4 to 13 times and reported as the mean of these analyses as $\delta^{57}Fe_{IRMM014}$ (the relative difference of $^{57}Fe/^{54}Fe$ between sample and reference standard IRMM014), subsequently abbreviated to $\delta^{57}Fe$ in the text. The uncertainty cited is two times the standard deviation (2 s.d.) of all the repeats. The analyses of the international rock standards yield values of $\delta^{57}Fe$ entirely consistent with previous studies (e.g., Weyer et al., 2005; Craddock et al., 2013; Williams and Bizimis, 2014), [Table S3]. Further analytical details of Fe isotope analyses are reported in the supplementary material.

4. Results

4.1. No fractionation by thermal diffusion

The analysis of four samples recovered at increasing distance from the pillow rim reveal insignificant variation in their Mg isotope ratios, from -0.236 ± 0.024 ‰ in the outer glassy sample to -0.266 ± 0.021 ‰ in the interior, micro-crystalline sample (Fig. 2c). As these values are not statistically distinguishable, there is no detectable Mg isotope fractionation across what would have been a marked, but short-lived, thermal gradient. As previously found for komatiites (Dauphas et al., 2010), we thus find no likely role for thermal diffusion in generating Mg isotopic variability MORB. The influence of thermal gradients on Fe isotope fractionation is generally much smaller compared to Mg isotope fractionation (Richter et al., 2009; Huang et al., 2010). From the absence of a detectable difference in Mg isotope composition between the glassy texture and micro-crystalline texture parts of the pillow margin section, we therefore conclude that Fe isotope fractionation driven by thermal diffusion is also likely to be negligible.

4.2. Mg and Fe isotopic compositions of MORB samples

The Mg isotope compositions of the MORB samples are given in Table 1 and displayed in Fig. 3a. In contrast to the previously documented homogeneous Mg isotopic composition of MORB (Teng et al., 2010), we observe Mg isotope differences, discernible with our higher precision. The samples from the EPR, MAR, and East Scotia Ridge exhibit similar $\delta^{26}Mg$, within uncertainty of a value of −0.210 ‰, while the samples from the Gakkel Ridge and SWIR display markedly lower Mg isotope ratios. Most samples from SEIR plot with the former group but one 'enriched' sample has anomalously low $\delta^{26}Mg$.

Furthermore, we obtain complementary variations in Fe isotope compositions, resulting in a striking inverse correlation of $\delta^{57}Fe$ with $\delta^{26}Mg$ (Fig. 4). Namely the EPR, MAR and all but the one 'enriched' sample from SEIR, have $\delta^{57}Fe$ values of approximately 0.1 ‰ (Fig. 3b and Table 1). However, the samples from the Gakkel Ridge, SWIR and the anomalous SEIR sample exhibit noticeably heavier Fe isotope compositions, up to approximately 0.25 ‰. It is worth noting that Richter et al. (2021) also reported markedly heavy Fe isotope compositions (up to approximately 0.28 ‰) in MORB samples from the Gakkel Ridge.

The two ridges that erupt MORB with distinctly lower $\delta^{26}Mg$ and higher $\delta^{57}Fe$ are remarkable for being ultra-slow spreading; the Gakkel Ridge and SWIR have full spreading rates of approximately 10 to 15 mm/year (Fig. 3), which have been argued to be sufficiently slow that the mantle up-welling beneath them is sub-adiabatic (e.g., Bown and White, 1994).

Although samples obtained from the back-arc East Scotia Ridge have been suggested to be influenced by subduction components (Fretzdorff et al., 2002), their Mg isotope ratios align with those of MORB samples originating from the EPR and MAR.

Table 1 also reports the $\Delta^{25}Mg'_{JP\text{-}1}$ value of ten MORB samples, which show a small range from 0.4 ± 1.0 ppm in a MAR sample to 2.9 ± 1.1 ppm in a Gakkel Ridge sample. In general, the samples from Gakkel ridge and SWIR have higher $\Delta^{25}Mg'_{JP\text{-}1}$ compared to the samples from EPR and MAR. A fertile peridotite sample, 314–56 from Vitim (Ionov 2004) was also measured relative to JP-1 and yielded $\Delta^{25}Mg'_{JP\text{-}1} = 1.4 \pm 1.2$ ppm and $\delta^{26}Mg'_{JP\text{-}1} = -0.015 \pm 0.033$ ‰.

5. Discussion

5.1. Mg isotope variations

5.1.1. Magma differentiation

Magma differentiation has the potential to induce small changes in the Mg isotope ratio of an evolving melt (Liu et al., 2022). Here, we assessed the effect of fractional crystallisation on Mg isotope ratios, following the simplified liquid line of descent depicted in Fig. 1a (see supplementary Table S6 for details of the calculation). The predicted variations are presented in Fig. 5a as a black arrow. The subtle increase in $\delta^{26}Mg$ with decreasing MgO observed in the samples from EPR, MAR, SEIR and Scotia Ridges are consistent with these modelling results, when selecting the $\delta^{26}Mg$ composition of primary melt as that of the least differentiated sample. This small increase of ~0.02 ‰ in $\delta^{26}Mg$ clearly cannot explain the low $\delta^{26}Mg$ in the samples from Gakkel Ridge and SWIR.

5.1.2. Mantle source and partial melting process

The analysis of mantle xenolith samples has consistently demonstrated that the accessible upper mantle possesses a homogeneous Mg isotope composition of approximately −0.24 ‰ ($\delta^{26}Mg$) (e.g., Teng

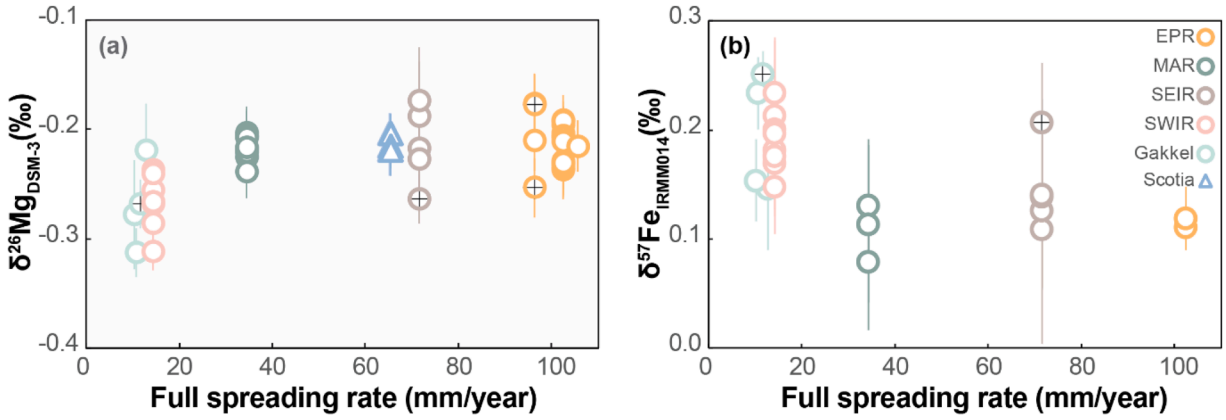

Fig. 3. (a) Magnesium isotope and (b) Fe isotope ratios of MORB plotted against the full spreading rates of the ridges from which they were erupted. Note the lower values of δ^{26}Mg and higher values of δ^{57}Fe in samples from the slowest spreading ridges. The spreading rate data are from Gale et al. (2013) for individual segments from which the samples were taken. `Enriched' samples are marked with crosses, see caption Fig. 1.

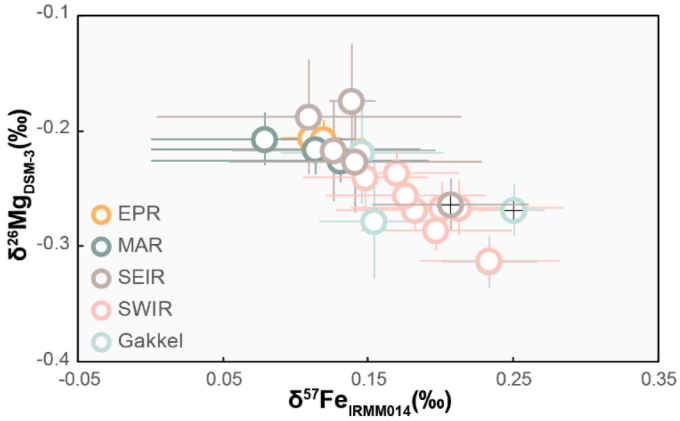

Fig. 4. Plot of δ^{26}Mg vs. δ^{57}Fe for MORB samples, showing a clear, negative co-variation. `Enriched' samples marked with crosses, see caption Fig. 1.

et al., 2013; Hin et al., 2017; Stracke et al., 2018; Liu et al., 2023). It has been shown that partial melting of peridotite could result in detectable Mg isotope fractionations of melt relative to its source (Stracke et al., 2018; Soderman et al., 2022), but estimates of this fractionation vary depending on the value chosen for the previously poorly constrained olivine-melt fractionation factor. Given a recent, higher precision determination of $\Delta^{26/24}$Mg $_{\text{Melt/Ol}}$ = 0.071 ‰ ± 0.010 at 1160 °C (Liu et al., 2022), Liu et al. (2023) calculated that melts derived by peridotite partial melting should exhibit δ^{26}Mg approximately 0.05 ‰ higher than their sources (i.e., around −0.19 ‰, Fig. 6) across a range of typical degrees of melting. This value is significantly higher than the values in samples from the ultra-slow spreading ridges and close to the highest δ^{26}Mg in our MORB.

5.2. Fe isotope variations

5.2.1. Magma differentiation

Fractional crystallisation is unlikely to account for the observed Fe isotope variations given the rather low experimentally determined equilibrium Fe isotope fractionation factors (Dauphas et al., 2014; Prissel et al., 2018). Schuessler et al. (2009) further showed the differentiation of basalt to basaltic andesite does not change the Fe isotope composition. In contrast, a recent study (Chen et al., 2019) empirically infers the role of fractional crystallisation to explain the elevated Fe isotope ratios in some markedly differentiated EPR MORB (MgO < 4 %). In Fig. 5b, we illustrate the resulting Fe isotope variations anticipated from this range of scenarios (see supplementary Table S6 for details). Firstly, we use the fractionation factors given in Dauphas et al. (2009, 2014), $\Delta^{57/54}$Fe $_{\text{Melt/Ol}}$ of 0.042 ‰ (assuming $Fe^{3+}/\Sigma Fe$ of 0.16; Cottrell and Kelley, 2011), derived from direct measurements of the force constant. In a second case we adopt a $\Delta^{57/54}$Fe $_{\text{Melt/Ol}}$ of 0.2 ‰, the value

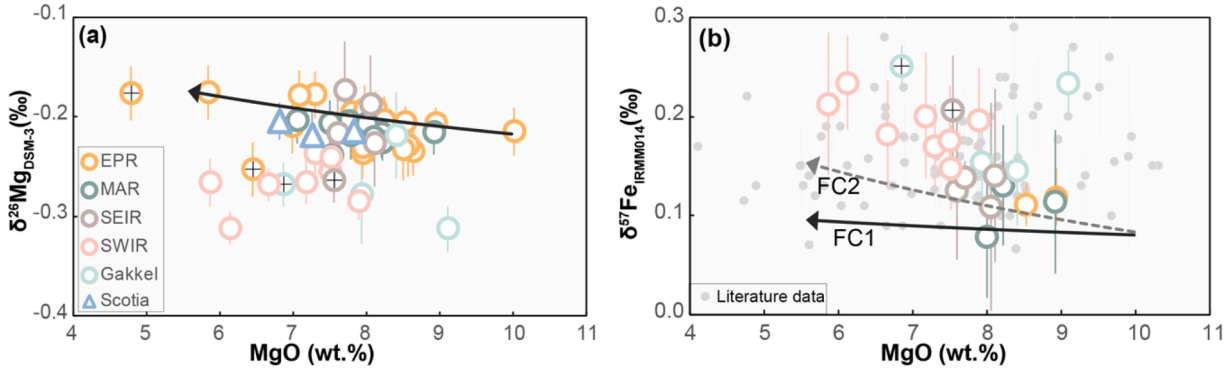

Fig. 5. (a) Mg isotope compositions and (b) Fe isotope composition of MORB analysed in this study (coloured symbols), plotted against MgO content. Literature Fe isotope data (faint grey circles) are from Weyer and Ionov (2007); Teng et al. (2013); Chen et al. (2019) and Richter et al. (2021). Literature data are not reported in (a) as they are significantly less precise and cannot resolve differences between samples. Black arrows show calculated isotope fractionation during magma differentiation. The two arrows for Fe isotope ratios represent the results adopting two different melt-solid fractionation factors, i.e., the solid line (FC1) is based on $\Delta^{57/54}$Fe $_{\text{Melt/Ol}}$ of 0.042 ‰, and the dashed line (FC2) is based on $\Delta^{57/54}$Fe $_{\text{Melt/Ol}}$ of 0.2 ‰; see Section 5.2.1 for more details. Neither reproduce the array of Fe isotope compositions. `Enriched' samples marked with crosses, see caption Fig. 1.

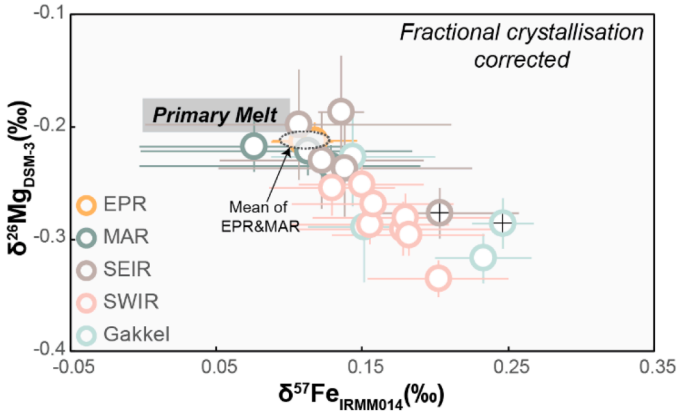

Fig. 6. Plot of δ^{26}Mg vs. δ^{57}Fe for MORB samples after correction for fractional crystallisation. This correction little changes the array relative to Fig. 4. The grey box indicates the peridicted range of δ^{26}Mg and δ^{57}Fe in equilibrium partial melts from peridotite, i.e. δ^{26}Mg between −0.175 ‰ and −0.205 ‰; δ^{57}Fe, between 0 and 0.1 ‰ (see Sections 5.1.2 and 5.2.2). The dashed ellipse represents the mean of the EPR and MAR samples, i.e. δ^{26}Mg of -0.212 ± 0.008 ‰ (2se) and δ^{57}Fe of 0.111 ± 0.017 ‰ (2se) and lies outside the grey box of predicted, primary equilibrium melt compositions. `Enriched' samples marked with crosses, see caption Fig. 1.

used by Chen et al. (2019). Neither model can reproduce the high δ^{57}Fe values observed in MORB from ultra-slow spreading ridges as a result of magmatic differentiation (Fig. 5b). A similar conclusion was drawn in a previous study of δ^{57}Fe in MORB from the Gakkel ridge (Richter et al., 2021).

We note that in apparent contradiction to the arguments above, there appears to be a correlation between decreasing MgO and δ^{57}Fe in Fig. 5b. However, this array dominantly reflects that in the limited subset of samples we analysed for Fe isotope ratios, those from the slowest spreading ridges had lower MgO (mainly from SWIR). Thus, we stress that the key observation is that samples with high δ^{57}Fe formed at slow spreading ridges, not that they have relatively low MgO.

5.2.2. Mantle source and partial melting process

Mounting evidence shows that the majority of peridotite samples have a limited range of near-chondritic Fe isotope compositions (δ^{57}Fe ~ -0.04 ‰) (Weyer et al., 2005; Schoenberg and von Blanckenburg, 2006; Weyer and Ionov, 2007; Dauphas et al., 2009; 2017; Craddock et al., 2013; Williams and Bizimis, 2014), while MORB samples have higher δ^{57}Fe ~0.15 ‰ (Weyer and Ionov, 2007; Craddock et al., 2013; Teng et al., 2013). This observation suggests that the heavier Fe isotope compositions observed in MORB samples are a result of the MORB formation process. While there is difficulty in obtaining the equilibrium Fe isotope fractionation factors between minerals (Dauphas et al., 2017), previous studies show that partial melts from peridotite could have δ^{57}Fe values between 0.04 to 0.14 ‰ higher than their sources (Dauphas et al., 2009; 2014; Williams and Bizimis, 2014; Soderman et al., 2021). Given δ^{57}Fe = −0.04 ‰ for mantle peridotite, predicted primary MORB should have a δ^{57}Fe ~ 0 to 0.1 ‰, which is slightly lower than the Fe isotope compositions of most EPR and MAR samples, and significantly lower than the values we obtained for the MORB samples from ultra-slow spreading ridges, i.e., Gakkel and SWIR (Fig. 5b).

The points discussed above are consolidated in Fig. 6, which shows samples corrected for the minor influence of fractional crystallisation (see supplementary material for details) plotted together with calculated primary melt compositions from peridotites (Sections 5.1.2 and 5.2.2). Samples from EPR, MAR, and SEIR (apart from the one anomalous, 'enriched' sample) plot closest to, but barely overlap with, the estimated primary melt compositions, while samples from the ultra-slow spreading Gakkel and SWIR form a negatively correlated array of δ^{26}Mg and δ^{57}Fe extending to values quite distinct from predicted, equilibrium mantle melt compositions.

5.3. Spreading rate control on diffusive fractionation of Mg and Fe isotope ratios

Although EPR, MAR, SEIR and the East Scotia Ridge have a range of spreading rates, they are all sufficiently high (>15 mm/year) to drive adiabatic decompression (e.g., Bown and White, 1994). If the mantle has similar potential temperatures beneath these ridges, they should undergo comparable degrees of melting producing similar crustal thicknesses and axial depths, as is generally observed (e.g., Klein and Langmuir, 1987). Beneath ultra-slow spreading centres, mantle is believed to upwell sub-adiabatically and as a result produces lower degree partial melts than beneath typical ridge segments, that then need to pass through a conductively cooled mantle 'lid' (Bown and White, 1994; Robinson et al., 2001). The fractionated Mg and Fe isotope compositions of melts erupted at ultra-slow spreading ridges seem linked to such contrasts in the partial melting process, but given the discussion in Sections 5.1 and 5.2, differences in equilibrium melt fractionation do not produce the expected compositions. Instead, we argue for the role of kinetic, diffusive fractionation during Mg-Fe exchange between melt and solid during melt transport to the surface, as briefly conceptualised by Liu et al. (2023) and expanded upon below.

In melting regimes beneath mid-ocean ridges, polybaric, fractional partial melting occurs (e.g., Klein and Langmuir, 1987). Deep melts from the bottom of the melting column might be out of equilibrium with the depleted harzburgite at the top of the melting column, with the melt being more Fe-rich and Mg-poor than equilibrium values. As deep melts pass through overlying depleted harzburgite there is thus a driving force for Mg-Fe exchange. Diffusionally limited, partial exchange of Fe from melt for Mg in the solid will result in isotopic fractionation. Isotopically lighter Fe preferentially diffuses from melt to solid and conversely isotopically light Mg preferentially diffuses from solid to melt. Thus, the δ^{57}Fe of the melt increases and its δ^{26}Mg decreases during its partial re-equilibration with peridotite en route to the surface. Where melt-solid ratios are smaller, as for smaller degrees of melting at ultra-slow spreading ridges, a given degree of re-equilibration results in a greater perturbation of melt isotope ratio. At slower spreading ridges, the mean melt velocity is also slower, providing more time for diffusive exchange. However, there does not appear to be a strong spreading rate dependence of Mg and Fe isotopic compositions at higher spreading rates (Fig. 3) suggesting that the melt-rock ratio is the dominant control in determining the amount of diffusive fractionation.

Given that isotopically heavy Mg and light Fe have been observed in the olivine phenocrysts of mafic magmas, it might be argued that removal of such crystals from the host magma during differentiation might be responsible for the anomalous compositions seen in the Gakkel Ridge and SWIR samples. However, this mechanism would predict low δ^{26}Mg in samples with low MgO, but for both the SWIR and Gakkel ridge the most MgO-rich sample has δ^{26}Mg as low or lower than the most MgO poor sample (Fig. 5a). Moreover, to generate melts with δ^{26}Mg systematically lower than equilibrium values requires interaction of melts with olivines that have Fe/Mg ratios lower than values for equilibrium element partitioning (Ulmer, 1989). This naturally occurs for melts traversing the harzburgitic mantle at the top of the melting column, but is not necessarily the case in crystal settling or magma mixing scenarios that lead to isotopically zoned phenocrysts. While magmatic differentiation processes may add to the kinetic fractionations seen in MORB, the relationship between δ^{26}Mg and δ^{57}Fe and spreading rate seems most readily explained by melt-rock interactions in the mantle.

5.4. A test of diffusive isotopic fractionation using the $\Delta^{25}Mg'$–$\delta^{26}Mg'$ plot

To test our hypothesis of diffusive isotopic fractionation, we need to distinguish this kinetic process from equilibrium isotopic fractionation, typically envisaged for mantle melting. This can be achieved using a

$\Delta^{25}Mg'$–$\delta^{26}Mg'$ diagram (Young and Galy, 2004), as we show for our MORB samples in Fig. 7. Given we calculated values of $\Delta^{25}Mg'_{JP\text{-}1}$ using an equilibrium fractionation law (Section 3.2), samples related by equilibrium fractionation should lie on a horizontal array. Moreover, as we have used the mantle peridotite JP-1 as our reference standard, if MORB melts were produced only by equilibrium melting and differentiation processes, their $\Delta^{25}Mg'_{JP\text{-}1}$ should be within error of zero (Fig. 7a). These expectations of equilibrium fractionation are not evident in the MORB samples plotted in Fig. 7b. Instead, the MORB data form a best-fitted slope of -0.010 ± 0.006 (2se), by York regression, identical with the theoretical slope of a kinetic process (Young and Galy, 2004). The dataset also passes a *t*-test ($\alpha = 0.05$) for the significance of the correlation. These observations strongly indicate that the Mg isotope ratios in the MORB samples are kinetically fractionated.

5.5. Source heterogeneity

The differences in $^{87}Sr/^{86}Sr$ between our MORB samples (Fig. 1b) show there must be some compositional variability between their sources. Thus, we also need to consider the potential influence of mantle heterogeneity on the Mg and Fe isotopic compositions of erupted MORB.

On a global scale there are no systematic differences in the $\delta^{26}Mg$ and $\delta^{57}Fe$ in samples from within and without the DUPAL anomaly, e.g. SEIR versus EPR samples (Fig. 8). This is readily rationalised in the context of the commonly invoked subduction origin of the DUPAL anomaly (Rehkaemper and Hofmann, 1997). Subduction can strongly influence the mantle budget of incompatible trace elements (e.g., elevating $^{87}Sr/^{86}Sr$) but negligibly affect $\delta^{26}Mg$, which is strongly buffered by the Mg-rich mantle (Liu et al., 2022). This point is further illustrated by our Scotia samples, which despite clear trace element signatures of subduction influence (Fretzdorff et al., 2002), have Mg isotopic compositions identical to non-subduction affected ridges like the EPR and MAR (Fig. 3a). Again, this reflects the large contrast in Mg contents between recycled crustal components and peridotites, so by mass balance it is difficult to perturb mantle $\delta^{26}Mg$ without creating unreasonable compositions in other elemental and isotopic systems (e.g., water contents and $^{143}Nd/^{144}Nd$, Liu et al., 2022).

It is well known that the MORB source can also show local 'enrichment' on a segment length scale. To focus on such variability, we have highlighted 4 samples (2 from EPR, 1 from SEIR and one from the Gakkel Ridge) which have significantly higher $^{87}Sr/^{86}Sr$ and $(La/Sm)_N$ relative to other samples from the same ridge (Fig. 1b). Three out of these 4 'enriched' samples have lower $\delta^{26}Mg$ and higher $\delta^{57}Fe$ (where measured) than other samples from the same ridge (Fig. 8). Interestingly they plot on the $\delta^{26}Mg$ versus $\delta^{57}Fe$ array (Fig. 6), suggesting they have experienced diffusive fractionation.

The 'enriched' SEIR sample (145-1) is unusual in that it was sampled close to the Australian-Antarctic discordance at greater depth (4665 m, Table. S1) than all but the SWIR samples. As such, it likely represents a low degree melt from a cooler mantle source (Klein and Langmuir, 1987; Klein et al., 1991) and so its low $\delta^{26}Mg$ and high $\delta^{57}Fe$ can be rationalised as due to a lower melt-rock ratio, as invoked for the ultra-slow spreading ridges. The other two 'enriched' samples with distinct $\delta^{26}Mg$ and $\delta^{57}Fe$ from other samples of the same ridge more clearly require a source control to explain their compositions. The enriched component evident in some MORB has been argued to be a component returned into the mantle by subduction and convective stirring, comprising either mafic crust (Prinzhofer et al., 1989) or small degree melts (Niu et al., 2002; Donnelly et al., 2004). Both cases juxtapose low and high Mg/Fe materials. Partial, diffusive Mg/Fe exchange in the solid state could result in the enriched component acquiring lower $\delta^{26}Mg$ and higher $\delta^{57}Fe$. This is admittedly a speculative suggestion from our very limited dataset. More work is required on enriched MORB to establish if they are systematically distinct in $\delta^{26}Mg$ and $\delta^{57}Fe$, although we note Sun et al. (2020) document elevated $\delta^{57}Fe$ for E-MORB from EPR.

We finally examine some previous suggestions of mantle source heterogeneity used to account for $\delta^{26}Mg$ and $\delta^{57}Fe$ variations of mantle derived melts in the context of our new measurements. The presence of pyroxenite in the melting source, has been invoked to explain the elevated $\delta^{57}Fe$ values in ocean island basalts (e.g., Soderman et al., 2021). Indeed, mantle pyroxenite samples have elevated $\delta^{57}Fe$ (up to 0.27 ± 0.050 ‰, Williams and Bizimis, 2014) and variable Mg isotope compositions from ~ −0.4 ‰ to ~0 ‰ ($\delta^{26}Mg$, Teng, 2017 and references therein). However, modelling calculations (Wang et al., 2020; Soderman et al., 2022; Liu et al., 2023) contradict the notion that partial melting of pyroxenite could generate melts with $\delta^{26}Mg$ as low as the values of −0.35 ‰ observed in our MORB. Melts derived from pyroxenites, instead, should have $\delta^{26}Mg$ elevated by ~0.1 ‰ relative to their sources (Wang et al., 2020; Soderman et al., 2022; Liu et al., 2023).

5.6. Implications

The offset between measured Mg and Fe isotope compositions of MORB and model predictions for partial melts of peridotite (Fig. 6)

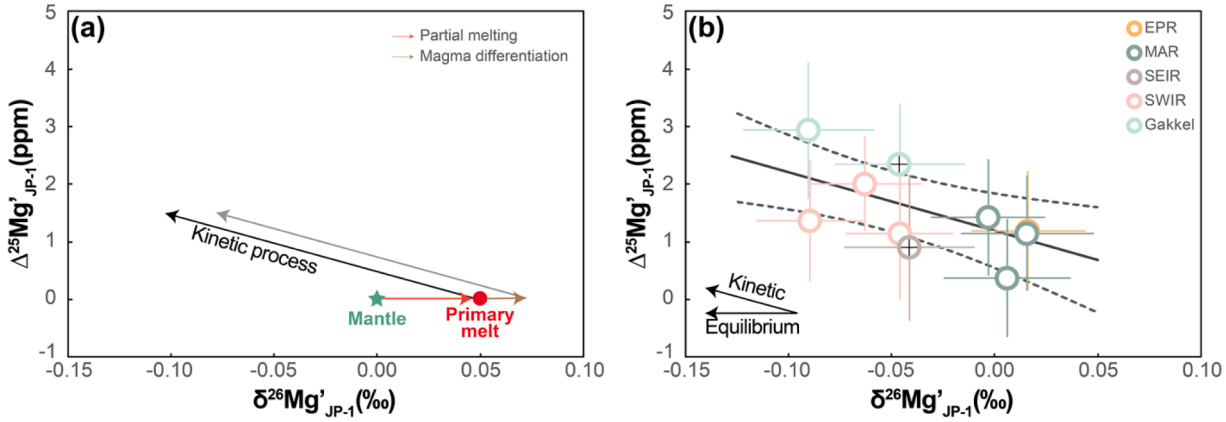

Fig. 7. (a) Illustration of MORB formation in a Δ'-δ' diagram for distinguishing equilibrium and kinetic processes. a) We assume partial melting and magma differentiation are equilibrium processes (horizontal lines). The magnitude of partial melt fractionation is from Liu et al. (2023) and the arrow for differentiation from this study (see Fig. 5a). A kinetically controlled process, such as diffusive Mg-Fe exchange produces a line with a slope of −0.01. (b) the Δ'-δ' diagram showing the MORB samples. The solid line is the best fit using a York regression and the two dashed lines indicate the 95 % confidence interval. The resulting slope is -0.010 ± 0.006 (2 s.e.), which is well within error of that produced by kinetic fractionation and resolved from the horizontal line predicted for equilibrium processes. Note in the figure all the Mg isotope data are reported against JP-1 instead of the default reference DSM-3 (see Section 5.4 for more details).The mantle value reference is from JP-1, in which represents the origin in the figures by definition. `Enriched' samples marked with crosses, see caption Fig. 1.

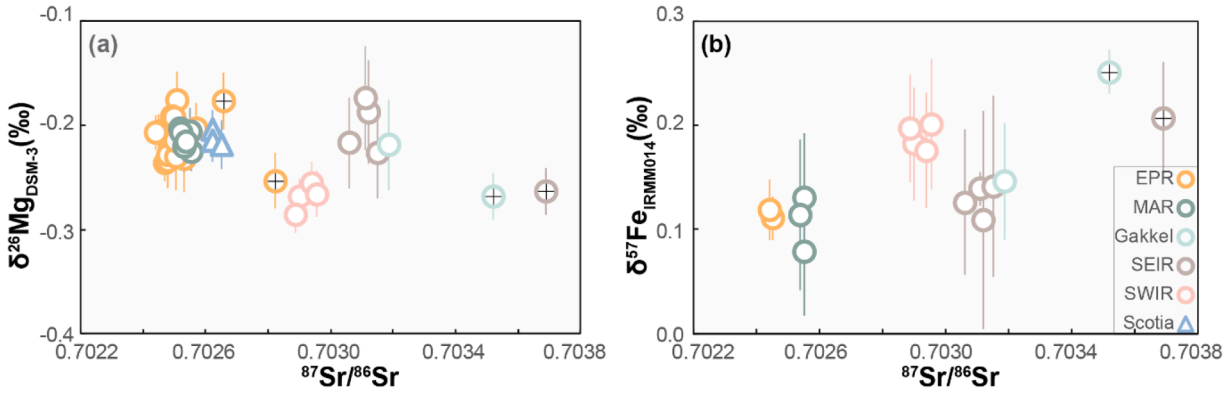

Fig. 8. (a) δ^{26}Mg and (b) δ^{57}Fe plotted against $^{87}Sr/^{86}Sr$. There are no systematic variations between Mg or Fe isotope compositions between samples from within the global DUPAL anomaly (SWIR and SEIR) and those without (EPR and MAR). `Enriched' samples marked with crosses, see caption Fig. 1. Some of these 'enriched' samples have lower δ^{26}Mg and higher δ^{57}Fe than other samples from the same ridge.

appears due to Mg-Fe inter-diffusion. This contention is strongly supported by the Δ'-δ' diagram which shows the MORB data form a linear line array with a slope of −0.01 (Fig. 7b) expected for kinetic fractionation. While the isotopic fractionation is more pronounced in the samples from the Gakkel Ridge and SWIR, even samples form EPR and MAR barely overlap with predicted primary melt compositions (Fig. 6). This implies that diffusive fractionation is ubiquitous during melt migration beneath ridges, even if it has a greater influence on magmas produced at ultra-slow spreading ridges with lower melt-solid ratios and a thickened, conductive lithospheric 'lid' (e.g., Robinson et al., 2001; Michael et al., 2003; Gale et al., 2013).

Modest differences between bulk Mg isotopic compositions of terrestrial peridotites and chondrites (0.02–0.06 ‰ in $\delta\delta^{26}$Mg, Hin et al., 2017) have been interpreted to reflect significant planetary evaporative loss of Mg (Hin et al., 2017, Young et al., 2019). Importantly, such differences are similar or smaller than the diffusive, Mg isotopic fractionations we observe in MORB (0.02 to 0.12 ‰ in δ^{26}Mg, Fig. 6). While recent, high precision analyses re-affirm a tightly constrained terrestrial δ^{26}Mg from peridotite analyses (Liu et al., 2023), the findings of this study show that the Mg isotopic composition of Earth's convecting mantle cannot be robustly determined from the analyses of its melts. This has important implications for trying to estimate the bulk compositions of other planetary objects that are only sampled by products of mantle derived melting (e.g. Mars, Moon, Vesta and the angrite parent body). The melting processes on such planetary bodies are poorly understood and may not result in conditions that would induce diffusive fractionation as identified in MORB formation on Earth, but this becomes an important potential consideration (e.g., Klaver et al., 2024).

The widespread occurrence of kinetic isotope fractionation in MORB samples also raises important questions regarding our understanding of terrestrial Mg and Fe stable isotope geochemistry. Over the past two decades, stable isotope ratios have been extensively used as a tool for tracing subduction recycled materials, identifying mantle heterogeneity, and investigating the signatures of the lower mantle (as reviewed in Teng et al., 2017). Most of these studies have assumed that observed, magmatic isotope fractionation reflects an equilibrium process, allowing it to be quantified with relative simplicity. This becomes much more difficult for kinetically limited processes, with a larger number of poorly constrained parameters influencing the final isotope ratio, even if there is the distant potential to understand rates of melt transport. Our study has demonstrated that kinetic isotope fractionation is prevalent in bulk magmatic samples, at least for the relatively fast inter-diffusion of Mg and Fe. Therefore, it is important to carefully assess the role of kinetic isotope fractionation before linking observed isotopic compositions in magmatic samples to their sources through equilibrium fractionation.

6. Conclusions

We have analysed the Mg and Fe isotope compositions of a wide range of MORB samples. Our findings reveal that samples from EPR, MAR, SEIR and the East Scotia Ridge have similar δ^{26}Mg ~ −0.210 ‰ and δ^{57}Fe of ~0.1 ‰, which are slightly isotopically lighter and heavier respectively than predicted primary MORB compositions of δ^{26}Mg of ~ −0.19 ‰ and δ^{57}Fe of ~0 to 0.1 ‰. Samples from the ultra-slow spreading Gakkel Ridge and SWIR have abnormally low Mg isotope ratios, down to ~ −0.320 ‰, and high δ^{57}Fe values, up to ~0.25 ‰. The negative co-variation of δ^{26}Mg and δ^{57}Fe and the fractionated Mg and Fe isotope compositions in MORB can be explained as a result of partial Mg-Fe exchange by inter-diffusion between melt and olivine during melt migration, as relatively Fe-rich melts travel to the surface and interact with depleted, Mg-rich residual harzburgite. The slope of MORB samples on a $\Delta^{25}Mg'_{JP-1}$-$\delta^{26}Mg'_{JP-1}$ diagram provides further evidence that Mg isotope fractionation is related to a kinetic process. Our findings suggest the widespread existence of kinetic stable isotope fractionations of Mg and Fe in modern MORB samples and likely other mantle derived melts.

CRediT authorship contribution statement

Xiao-Ning : Writing – review & editing, Writing – original draft, Methodology, Investigation, Formal analysis, Data curation, Conceptualization. **Remco C. Hin:** Writing – review & editing, Methodology, Funding acquisition, Conceptualization. **Christopher D. Coath:** Writing – review & editing, Methodology, Investigation. **Tim Elliott:** Writing – review & editing, Supervision, Resources, Project administration, Funding acquisition, Conceptualization.

Declaration of competing interest

The authors declare that they have no known competing financial interests or personal relationships that could have appeared to influence the work reported in this paper.

Data availability

Data will be made available on request.

Acknowledgements

David W. Graham, Katherine Kelley, Yaoling Niu, C.J. Robinson and Dimitri Ionov are thanked for providing the MORB and peridotite samples. Constructive comments from C.K. Sio and another anonymous reviewer were of great help when improving this manuscript. This work

was funded by ERC Adv Grant 883351 NONUNE building on work from NERC grant NE/LOO7428/1. Xiao-Ning Liu was partly financially supported by a CSC-UOB joint scholarship (China Scholarship Council - University of Bristol) during this work. Remco C. Hin was partly supported by ERC Starting Grant 949417 VapLoss.

Supplementary materials

Supplementary material associated with this article can be found, in the online version, at doi:10.1016/j.epsl.2024.118868.

References

Bown, J.W., White, R.S., 1994. Variation with spreading rate of oceanic crustal thickness and geochemistry. Earth Planet. Sci. Lett. 121, 435–449.
Chen, S., Niu, Y., Guo, P., Gong, H., Sun, P., Xue, Q., Duan, M., Wang, X., 2019. Iron isotope fractionation during mid-ocean ridge basalt (MORB) evolution: evidence from lavas on the East Pacific Rise at 10 30′ N and its implications. Geochim. Cosmochim. Acta 267, 227–239.
Coath, C.D., Elliott, T., Hin, R.C., 2017. Double-spike inversion for three-isotope systems. Chem. Geol. 451, 78–89.
Cottrell, E., Kelley, K.A., 2011. The oxidation state of Fe in MORB glasses and the oxygen fugacity of the upper mantle. Earth Planet. Sci. Lett. 305, 270–282.
Craddock, P.R., Warren, J.M., Dauphas, N., 2013. Abyssal peridotites reveal the near-chondritic Fe isotopic composition of the Earth. Earth Planet. Sci. Lett. 365, 63–76.
Dauphas, N., Craddock, P.R., Asimow, P.D., Bennett, V.C., Nutman, A.P., Ohnenstetter, D., 2009. Iron isotopes may reveal the redox conditions of mantle melting from Archean to present. Earth Planet. Sci. Lett. 288, 255–267.
Dauphas, N., John, S.G., Rouxel, O., 2017. Iron isotope systematics. Rev. Mineral. Geochem. 82, 415–510.
Dauphas, N., Roskosz, M., Alp, E.E., Neuville, D.R., Hu, M.Y., Sio, C.K., Tissot, F.L.H., Zhao, J., Tissandier, L., Médard, E., Cordier, C., 2014. Magma redox and structural controls on iron isotope variations in Earth's mantle and crust. Earth Planet. Sci. Lett. 398, 127–140.
Dauphas, N., Teng, F.-Z., Arndt, N.T., 2010. Magnesium and iron isotopes in 2.7 Ga Alexo komatiites: mantle signature, no evidence for Soret diffusion, and identification of diffusive transport in zoned olivine. Geochim. Cosmochim. Acta 74, 3274–3291.
Donnelly, K.E., Goldstein, S.L., Langmuir, C.H., Spiegelman, M., 2004. Origin of enriched ocean ridge basalts and implications for mantle dynamics. Earth Planet. Sci. Lett. 226, 347–366.
Dupré, B., Allégre, C.J., 1983. Pb–Sr isotope variations in Indian Ocean basalts and mixing phenomena. Nature 303, 142–146.
Fretzdorff, S., Livermore, R.A., Devey, C.W., Leat, P.T., Stoffers, P., 2002. Petrogenesis of the back-arc east scotia ridge, south Atlantic ocean. J. Petrol. 43, 1435–1467.
Gale, A., Dalton, C.A., Langmuir, C.H., Su, Y., Schilling, J.G., 2013. The mean composition of ocean ridge basalts. Geochem. Geophys. Geosyst. 14, 489–518.
Gregory, T., Luu, T.H., Coath, C.D., Russell, S.S., Elliott, T., 2020. Primordial formation of major silicates in a protoplanetary disc with homogeneous $^{26}Al/^{27}Al$. Sci. Adv. 6, eaay9626.
Hart, S.R., 1984. A large-scale isotope anomaly in the southern hemisphere mantle. Nature 309, 753–757.
Hin, R.C., Coath, C.D., Carter, P.J., Nimmo, F., Lai, Y.-J., Pogge von Strandmann, P.A.E., Willbold, M., Leinhardt, Z.M., Walter, M.J., Elliott, T., 2017. Magnesium isotope evidence that accretional vapour loss shapes planetary compositions. Nature 549, 511–515.
Huang, F., Chakraborty, P., Lundstrom, C.C., Holmden, C., Glessner, J.J.G., Kieffer, S.W., Lesher, C.E., 2010. Isotope fractionation in silicate melts by thermal diffusion. Nature 464, 396–400.
Ionov, D., 2004. Chemical variations in peridotite xenoliths from Vitim, Siberia: inferences for REE and Hf behaviour in the garnet-facies upper mantle. J. Petrol. 45, 343–367.
Klaver, M., Klemme, S., Liu, X.-N., Hin, R.C., Coath, C.D., Anand, M., Lissenberg, C.J., Berndt, J., Elliott, T., 2024. Titanium-rich basaltic melts on the Moon modulated by reactive flow processes. Nat. Geosci. 17, 118–123.
Klein, E.M., Langmuir, C.H., 1987. Global correlations of ocean ridge basalt chemistry with axial depth and crustal thickness. J. Geophys. Res. Solid Earth 92, 8089–8115.
Klein, E.M., Langmuir, C.H., Staudigel, H., 1991. Geochemistry of basalts from the southeast Indian ridge, 115 E–138 E. J. Geophys. Res. Solid Earth 96, 2089–2107.
Liu, X.-N., Hin, R.C., Coath, C.D., Bizimis, M., Su, L., Ionov, D.A., Takazawa, E., Brooker, R., Elliott, T., 2023. The magnesium isotopic composition of the mantle. Geochim. Cosmochim. Acta 358, 12–26.
Liu, X.N., Hin, R.C., Coath, C.D., van Soest, M., Melekhova, E., Elliott, T., 2022. Equilibrium olivine-melt Mg isotopic fractionation explains high δ26Mg values in arc lavas. Geochem. Perspect. Lett. 22, 42–47.
Luu, T.H., Hin, R.C., Coath, C.D., Elliott, T., 2019. Bulk chondrite variability in mass independent magnesium isotope compositions–implications for initial solar system $^{26}Al/^{27}Al$ and the timing of terrestrial accretion. Earth Planet. Sci. Lett. 522, 166–175.
Mahoney, J.J., Graham, D.W., Christie, D.M., Johnson, K.T.M., Hall, L.S., Vonderhaar, D. L., 2002. Between a hotspot and a cold spot: isotopic variation in the Southeast Indian Ridge asthenosphere, 86°E–118°E. J. Petrol. 43, 1155–1176.
Michael, P.J., Langmuir, C.H., Dick, H.J.B., Snow, J.E., Goldstein, S.L., Graham, D.W., Lehnert, K., Kurras, G., Jokat, W., Mühe, R., Edmonds, H.N., 2003. Magmatic and amagmatic seafloor generation at the ultraslow-spreading Gakkel ridge, Arctic ocean. Nature 423, 956–961.
Niu, Y., Batiza, R., 1994. Magmatic processes at a slow spreading ridge segment: 26°S Mid-Atlantic ridge. J. Geophys. Res. Solid Earth 99, 19719–19740.
Niu, Y., Collerson, K.D., Batiza, R., Wendt, J.I., Regelous, M., 1999. Origin of enriched-type mid-ocean ridge basalt at ridges far from mantle plumes: the East Pacific Rise at 11°20′ N. J. Geophys. Res. Solid Earth 104, 7067–7087.
Niu, Y., Regelous, M., Wendt, I.J., Batiza, R., O'Hara, M.J., 2002. Geochemistry of near-EPR seamounts: importance of source vs. process and the origin of enriched mantle component. Earth Planet. Sci. Lett. 199, 327–345.
Niu, Y., Waggoner, D.G., Sinton, J.M., Mahoney, J.J., 1996. Mantle source heterogeneity and melting processes beneath seafloor spreading centers: the East Pacific Rise, 18–19°S. J. Geophys. Res. Solid Earth 101, 27711–27733.
Oeser, M., Dohmen, R., Horn, I., Schuth, S., Weyer, S., 2015. Processes and time scales of magmatic evolution as revealed by Fe–Mg chemical and isotopic zoning in natural olivines. Geochim. Cosmochim. Acta 154, 130–150.
Palme, H., O'Neill, H., 2014. Cosmochemical estimates of mantle composition. In: Holland, H.D., Turekian, K.K. (Eds.), Treatise on Geochemistry, second ed. Elsevier, Oxford, pp. 1–39.
Poitrasson, F., Delpech, G., Grégoire, M., 2013. On the iron isotope heterogeneity of lithospheric mantle xenoliths: implications for mantle metasomatism, the origin of basalts and the iron isotope composition of the Earth. Contrib. Mineral. Petrol. 165, 1243–1258.
Prinzhofer, A., Lewin, E., Allegre, C.J., 1989. Stochastic melting of the marble cake mantle: evidence from local study of the East Pacific Rise at 12° 50′ N. Earth Planet. Sci. Lett. 92, 189–206.
Prissel, K.B., Krawczynski, M.J., Nie, N.X., Dauphas, N., Couvy, H., Hu, M.Y., Alp, E.E., Roskosz, M., 2018. Experimentally determined effects of olivine crystallization and melt titanium content on iron isotopic fractionation in planetary basalts. Geochim. Cosmochim. Acta 238, 580–598.
Regelous, M., Niu, Y., Wendt, J.I., Batiza, R., Greig, A., Collerson, K.D., 1999. Variations in the geochemistry of magmatism on the East Pacific Rise at 10°30′ N since 800 ka. Earth Planet. Sci. Lett. 168, 45–63.
Regelous, M., Niu, Y., Abouchami, W., Castillo, P.R., 2009. Shallow origin for South Atlantic Dupal Anomaly from lower continental crust: geochemical evidence from the Mid-Atlantic ridge at 26°S. Lithos 112, 57–72.
Rehka, M., Hofmann, A.W., 1997. Recycled ocean crust and sediment in Indian ocean MORB. Earth Planet. Sci. Lett. 147, 93–106.
Richter, F.M., Watson, E.B., Mendybaev, R.A., Teng, F.Z., Janney, P.E., 2008. Magnesium isotope fractionation in silicate melts by chemical and thermal diffusion. Geochim. Cosmochim. Acta 72, 206–220.
Richter, F.M., Watson, E.B., Mendybaev, R., Dauphas, N., Georg, B., Watkins, J., Valley, J., 2009. Isotopic fractionation of the major elements of molten basalt by chemical and thermal diffusion. Geochim. Cosmochim. Acta 73, 4250–4263.
Richter, M., Nebel, O., Schwindinger, M., Nebel-Jacobsen, Y., Dick, H.J., 2021. Competing effects of spreading rate, crystal fractionation and source variability on Fe isotope systematics in mid-ocean ridge lavas. Sci. Rep. 11, 4123.
Richter, M., Nebel, O., Maas, R., Mather, B., Nebel-Jacobsen, Y., Capitanio, F.A., Dick, H. J., Cawood, P.A., 2020. An early cretaceous subduction-modified mantle underneath the ultraslow spreading Gakkel ridge, Arctic ocean. Sci. Adv. 6, eabb4340.
Robinson, C.J., Bickle, M.J., Minshull, T.A., White, R.S., Nichols, A.R.L., 2001. Low degree melting under the southwest Indian ridge: the roles of mantle temperature, conductive cooling and wet melting. Earth Planet. Sci. Lett. 188, 383–398.
Robinson, C.J., White, R.S., Bickle, M.J., Minshull, T.A., 1996. Restricted melting under the very slow-spreading southwest Indian ridge. In: MacLeod, C.J., Tyler, P.A., Walker, C.L. (Eds.), Tectonic, Magmatic, Hydrothermal and Biological Segmentation of Mid-Ocean Ridges, Spec. Publ., 118. Geol. Soc. London, pp. 131–141.
Schoenberg, R., von Blanckenburg, F., 2006. Modes of planetary-scale Fe isotope fractionation. Earth Planet. Sci. Lett. 252, 342–359.
Schuessler, J.A., Schoenberg, R., Sigmarsson, O., 2009. Iron and lithium isotope systematics of the Hekla volcano, Iceland—Evidence for Fe isotope fractionation during magma differentiation. Chem. Geol. 258, 78–91.
Sims, K.W., Goldstein, S.J., Blichert-Toft, J., Perfit, M.R., Kelemen, P., Fornari, D.J., Michael, P., Murrell, M.T., Hart, S.R., DePaolo, D.J., Layne, G., 2002. Chemical and isotopic constraints on the generation and transport of magma beneath the East Pacific Rise. Geochim. Cosmochim. Acta 66, 3481–3504.
Sio, C.K.I., Dauphas, N., Teng, F.-Z., Chaussidon, M., Helz, R.T., Roskosz, M., 2013. Discerning crystal growth from diffusion profiles in zoned olivine by in situ Mg–Fe isotopic analyses. Geochim. Cosmochim. Acta 123, 302–321.
Soderman, C.R., Matthews, S., Shorttle, O., Jackson, M.G., Ruttor, S., Nebel, O., Turner, S., Beier, C., Millet, M.A., Widom, E., Humayun, M., 2021. Heavy $\delta^{57}Fe$ in ocean island basalts: a non-unique signature of processes and source lithologies in the mantle. Geochim. Cosmochim. Acta 292, 309–332.
Soderman, C.R., Shorttle, O., Matthews, S., Williams, H.M., 2022. Global trends in novel stable isotopes in basalts: theory and observations. Geochim. Cosmochim. Acta 318, 388–414.
Stracke, A., Tipper, E.T., Klemme, S., Bizimis, M., 2018. Mg isotope systematics during magmatic processes: inter-mineral fractionation in mafic to ultramafic Hawaiian xenoliths. Geochim. Cosmochim. Acta 226, 192–205.
Sun, P., Niu, Y., Guo, P., Duan, M., Chen, S., Gong, H., Wang, X., Xiao, Y., 2020. Large iron isotope variation in the eastern Pacific mantle as a consequence of ancient low-degree melt metasomatism. Geochim. Cosmochim. Acta 286, 269–288.
Teng, F.Z., 2017. Magnesium isotope geochemistry. Rev. Mineral. Geochem. 82, 219–287.

Teng, F.-Z., Dauphas, N., Helz, R.T., Gao, S., Huang, S., 2011. Diffusion-driven magnesium and iron isotope fractionation in Hawaiian olivine. Earth Planet. Sci. Lett. 308, 317–324.
Teng, F.Z., Dauphas, N., Huang, S., Marty, B., 2013. Iron isotopic systematics of oceanic basalts. Geochim. Cosmochim. Acta 107, 12–26.
Teng, F.-Z., Li, W.-Y., Ke, S., Marty, B., Dauphas, N., Huang, S., Wu, F.-Y., Pourmand, A., 2010. Magnesium isotopic composition of the Earth and chondrites. Geochim. Cosmochim. Acta 74, 4150–4166.
Teng, F.-Z., Wadhwa, M., Helz, R.T., 2007. Investigation of magnesium isotope fractionation during basalt differentiation: implications for a chondritic composition of the terrestrial mantle. Earth Planet. Sci. Lett. 261, 84–92.
Teng, F.Z., Watkins, J., Dauphas, N. (Eds.), 2017. Non-traditional Stable Isotopes. The Mineralogical Society of America, Virginia. https://doi.org/10.2138/rmg.2017.82.0.
Ulmer, P., 1989. The dependence of the Fe^{2+}–Mg cation-partitioning between olivine and basaltic liquid on pressure, temperature and composition. Contrib. Mineral. Petrol. 101, 261–273.
Wang, Y., He, Y.-S., Ke, S., 2020. Mg isotope fractionation during partial melting of garnet-bearing sources: an adakite perspective. Chem. Geol. 537, 119478.
Weyer, S., Anbar, A.D., Brey, G.P., Münker, C., Mezger, K., Woodland, A.B., 2005. Iron isotope fractionation during planetary differentiation. Earth Planet. Sci. Lett. 240, 251–264.
Weyer, S., Ionov, D.A., 2007. Partial melting and melt percolation in the mantle: the message from Fe isotopes. Earth Planet. Sci. Lett. 259, 119–133.
Williams, H.M., Bizimis, M., 2014. Iron isotope tracing of mantle heterogeneity within the source regions of oceanic basalts. Earth Planet. Sci. Lett. 404, 396–407.
Young, E.D., Galy, A., 2004. The isotope geochemistry and cosmochemistry of magnesium. Rev. Mineral. Geochem. 55, 197–230.
Young, E.D., Shahar, A., Nimmo, F., Schlichting, H.E., Schauble, E.A., Tang, H., Labidi, J., 2019. Near-equilibrium isotope fractionation during planetesimal evaporation. Icarus 323, 1–15.